J Biomol NMR (2014) 60:203–208
DOI 10.1007/s10858-014-9868-5

COMMUNICATION

Triple resonance-based $^{13}C^{\alpha}$ and $^{13}C^{\beta}$ CEST experiments for studies of ms timescale dynamics in proteins

Dong Long · Ashok Sekhar · Lewis E. Kay

Received: 15 August 2014 / Accepted: 13 October 2014 / Published online: 28 October 2014

Abstract A pair of triple resonance based CEST pulse schemes are presented for measuring $^{13}C^{\alpha}$ and $^{13}C^{\beta}$ chemical shifts of sparsely populated and transiently formed conformers that are invisible to traditional NMR experiments. CEST profiles containing dips at resonance positions of $^{13}C^{\alpha}$ or $^{13}C^{\beta}$ spins of major (ground) and minor (excited) conformers are obtained in a pseudo 3rd dimension that is generated by quantifying modulations of cross peaks in ^{15}N, $^{1}H^{N}$ correlation spectra. An application to the folding reaction of a G48A mutant of the Fyn SH3 domain is presented, illustrating and validating the methodology.

Keywords CEST · Conformationally excited protein states · $^{13}C^{\alpha/\beta}$ chemical shifts · Chemical exchange · Fyn SH3 · Protein folding

A major strength of NMR spectroscopy derives from the ability to manipulate spin systems in a variety of different ways to extract the rich chemical information that is encoded in a wide range of measurable parameters (Cavanagh et al. 1996; Ernst et al. 1987). A case in point emerges in the context of triple resonance multidimensional NMR experiments that are used for resonance assignment (Bax and Grzesiek 1993; Clore and Gronenborn 1991; Sattler et al. 1999). Here different pathways of magnetization transfer are exploited in the acquisition of each spectrum to obtain a series of correlated chemical shifts with some redundancy between data sets. The redundancy is then used to link chemical shifts and, thus, assign peaks to residue specific positions in the biomolecule. The ability to extract information reported by a particular site using potentially multiple approaches becomes critical in cases where overlap or sensitivity is problematic. For example, a standard experiment for recording ^{13}C chemical shifts in biomolecular NMR spectroscopy is the constant-time (CT) ^{13}C–^{1}H HSQC (Santoro and King 1992; Vuister and Bax 1992), yet peak overlap is often an issue, especially for larger molecules. In this context improved resolution can be obtained using triple resonance experiments which correlate carbon or proton shifts with those from ^{15}N, $^{1}H^{N}$ amide spin pairs (Grzesiek et al. 1993; Montelione et al. 1992). Information carried by ^{13}C and ^{1}H nuclei can thus be obtained, even if their positions cannot be resolved in the ^{13}C–^{1}H spectrum.

In this communication we present a pair of amide-detected triple resonance experiments for recording millisecond time-scale dynamics at $^{13}C^{\alpha}$ and $^{13}C^{\beta}$ sites in uniformly ^{15}N, ^{13}C labeled proteins. The experiments follow closely our recently published ^{13}C–^{1}H HSQC-based approach for studying conformational exchange involving protein side-chains using Chemical Exchange Saturation Transfer (CEST) (Bouvignies et al. 2014). The triple resonance versions of the experiments provide improved resolution, and, no interference from the residual water line that can be an issue for quantification of $^{13}C^{\alpha}$–$^{1}H^{\alpha}$ correlations in cases where the resonance positions of the $^{1}H^{\alpha}$ and water protons are nearly degenerate. The methodology is demonstrated on a G48A mutant Fyn SH3 domain that interconverts between

Electronic supplementary material The online version of this article (doi:10.1007/s10858-014-9868-5) contains supplementary material, which is available to authorized users.

D. Long · A. Sekhar · L. E. Kay (✉)
Departments of Molecular Genetics, Biochemistry and Chemistry, The University of Toronto, Toronto, ON M5S 1A8, Canada
e-mail: kay@pound.med.utoronto.ca

L. E. Kay
Program in Molecular Structure and Function, Hospital for Sick Children, 555 University Avenue, Toronto, ON M5G 1X8, Canada

NMR observable native (N) and 'invisible' unfolded (U) states (Bouvignies et al. 2014). Excellent agreement is obtained between $^{13}C^{\alpha}/^{13}C^{\beta}$ chemical shifts of the U state using either ^{13}C–^{1}H HSQC or triple resonance approaches.

Figure 1a shows the $^{13}C^{\alpha}$ CEST-based pulse scheme that records $^{13}C^{\alpha}$ chemical shifts indirectly via intensity modulations of cross peaks in a series of ^{15}N, $^{1}H^{N}$ correlation spectra. In the parlance of triple resonance spectroscopy the experiment can be termed an (HACACO)NNH and is similar to a class of pulse schemes used for backbone resonance assignment of ^{15}N, ^{13}C labeled proteins (Grzesiek and Bax 1992, 1993), with the magnetization flow schematically given by

$$^{1}H^{\alpha} \xrightarrow{J_{CH}} {}^{13}C^{\alpha} CEST(B_1) \xrightarrow{J_{C\alpha CO}} {}^{13}CO \xrightarrow{J_{CON}} {}^{15}N(t_1) \xrightarrow{J_{NH}} {}^{1}H_N(t_2). \quad (1)$$

In Eq. (1) the active couplings in the transfer process are indicated above the arrows and t_1, t_2 denote acquisition times. A series of ^{15}N, $^{1}H^{N}$ planes is thus obtained, recorded as a function of the position of the weak ^{13}C B_1 field (typically between 15 and 50 Hz) that spans the range of $^{13}C^{\alpha}$ chemical shifts one plane at a time. By plotting the intensity of each amide cross-peak versus B_1 position a pseudo 3rd (CEST) dimension is generated, whereby in each profile a large dip at the $^{13}C^{\alpha}$ position of the major state (N) and a smaller dip centered at the $^{13}C^{\alpha}$ resonance frequency of the minor conformer (U in this case) is observed. In the scheme of Fig. 1a the delay τ_b is set to $0.25/J_{CH}$ to achieve optimal signal to noise for methine carbons (i.e., all $^{13}C^{\alpha}$ with the exception of Gly) and the methylene groups from Gly residues give little signal. Because the Gly $^{13}C^{\alpha}$ carbons resonate uniquely upfield of the remaining $^{13}C^{\alpha}$ spins, a separate optimal data set can be recorded for this residue with no increase in measurement time. This is achieved with τ_b set to $0.125/J_{CH}$ and focusing on a region in the CEST dimension extending from approximately 42–48 ppm.

It is also possible to design a similar sequence to generate $^{13}C^{\beta}$ CEST profiles recorded as a series of modulated ^{15}N, $^{1}H^{N}$ planes. Figure 1b illustrates the scheme that has been used, based on the popular (HB)CBCA(CO)NNH sequence (Grzesiek and Bax 1992). The magnetization transfer can be summarized as,

$$^{1}H^{\alpha/\beta} \xrightarrow{J_{CH}} {}^{13}C^{\alpha/\beta} CEST(B_1) \longrightarrow {}^{13}C^{\beta} \xrightarrow{J_{C\beta C\alpha}} {}^{13}C^{\alpha} \xrightarrow{J_{C\alpha CO}} {}^{13}CO \xrightarrow{J_{CON}} {}^{15}N(t_1) \xrightarrow{J_{NH}} {}^{1}H_N(t_2). \quad (2)$$

A number of features, unique to this experiment, are noteworthy. First, unlike the $^{13}C^{\alpha}$ CEST experiment described above, where optimal data sets can be recorded for methine and methylene groups without an increase in net measurement time, a more complex situation emerges for the $^{13}C^{\beta}$ CEST scheme because chemical shifts for the Ile and Val methine C^{β} carbons can be similar to those for methylene $^{13}C^{\beta}$ spins. Here we have optimized for methylenes ($\tau_b = 0.125/J_{CH}$), with 70 % of maximum sensitivity obtained for methines (Ile,Val). In principle, the distinct resonance frequencies for Thr $^{13}C^{\beta}$ permit recording an optimal data set for this amino acid with no increase in measurement time by doubling τ_b. A second issue results from the fact that the CEST data is recorded as a set of ^{15}N, $^{1}H^{N}$ spectra, so that a priori it is not possible to distinguish between magnetization originating on $^{13}C^{\beta}$ or $^{13}C^{\alpha}$ since transfer pathways from both $^{1}H^{\beta}/^{13}C^{\beta}$ and $^{1}H^{\alpha}/^{13}C^{\alpha}$ pairs of spins are allowed in the standard (HB)CBCA(CO)NNH experiment. Indeed, correlating both $^{13}C^{\beta}$ and $^{13}C^{\alpha}$ chemical shifts with backbone amides has been shown to be extremely powerful for the assignment of protein resonances (Grzesiek and Bax 1992; Wittekind and Mueller 1993). In the present application, the presence of both magnetization transfer pathways is less desirable, however, since the $^{13}C^{\beta}$ pathway carries the information of interest, while magnetization from $^{13}C^{\alpha}$ is never modulated as a function of the B_1 field and hence leads only to an offset in each profile that depends on the relaxation properties of the $^{13}C^{\alpha}$ spin in question. In principle the offset can be included in analysis of the data by introducing an additional fitting parameter, however we prefer to eliminate the signal from the $^{13}C^{\alpha}$ spin experimentally by recording successive scans with and without the $^{13}C^{\alpha}$ selective inversion pulse (green) in Fig. 1b. In this manner magnetization that results from a transfer process involving $^{13}C^{\alpha}$ inverts sign in successive scans while signal from $^{13}C^{\beta}$ does not. Addition of scans, therefore, preserves the signal of interest while eliminating the $^{13}C^{\alpha}$ path.

Figure 2a shows a portion of the 2D ^{15}N, $^{1}H^{N}$ HSQC plane recorded on a sample of the G48A Fyn SH3 domain, a module that has been shown previously to interconvert between native and unfolded states, $N \underset{k_{UN}}{\overset{k_{NU}}{\rightleftarrows}} U$, with an exchange rate $k_{ex} \sim 140\ s^{-1}$, 25 °C, pH = 7 (Bouvignies et al. 2014; Long et al. 2014). The amide correlation of a given residue encodes the $^{13}C^{\alpha}$, or in the case of scheme 1B the $^{13}C^{\beta}$, chemical shift of the preceding residue of both ground and excited state conformers. Figure 2b illustrates CEST profiles for a number of $^{13}C^{\alpha}/^{13}C^{\beta}$ spins recorded using a weak B_1 field of approximately 25 Hz, color-coded to match the correlations in the amide spectrum from which they derive. As shown here, separate CEST dips were observed in many cases for both $^{13}C^{\alpha}$ and $^{13}C^{\beta}$ spins of ground and excited states, as might be expected when large conformational changes are involved in the exchange process. Notably, ^{13}C–^{13}C couplings are not visible in any of the recorded CEST profiles, despite the fact that U–^{13}C samples are used in this class of experiment. As observed previously

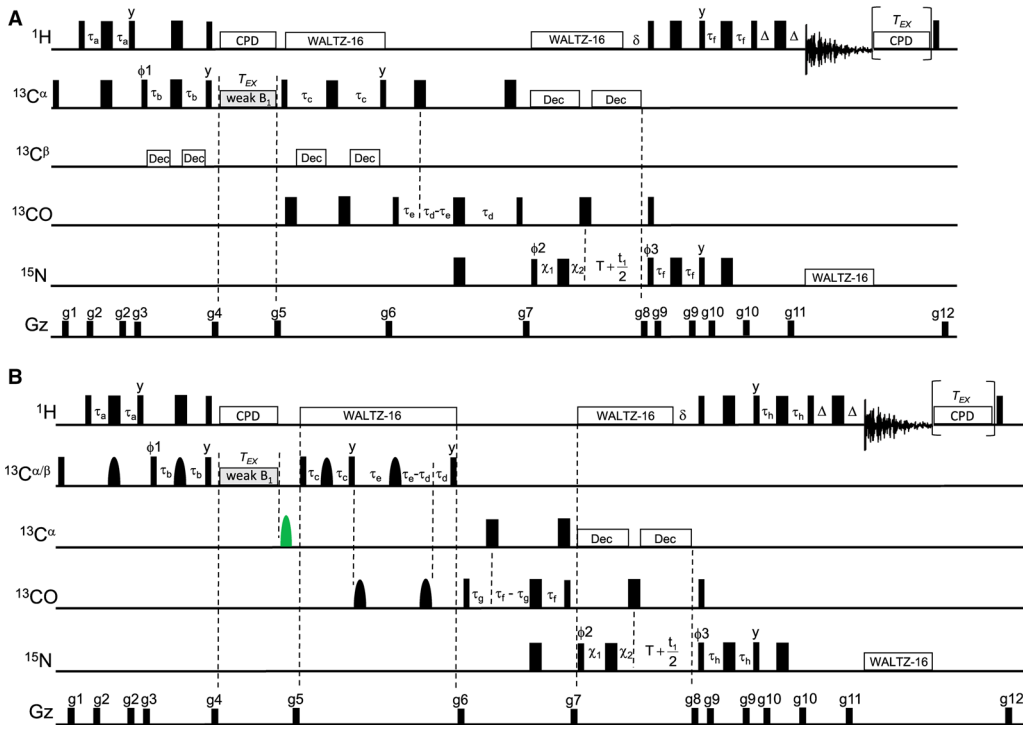

Fig. 1 Pulse schemes for (**a**) HACACONNH-CEST ($^{13}C^{\alpha}$) and (**b**) HBCBCACONNH-CEST ($^{13}C^{\beta}$). Narrow and wide rectangles correspond to 90° and 180° pulses, respectively, applied along the *x*-axis unless otherwise indicated. ^{1}H decoupling is achieved using a 6 kHz WALTZ-16 decoupling element (Shaka et al. 1983), except during the CEST delay of duration T_{EX} where a composite pulse scheme, $90_x240_y90_x$ (Levitt and Freeman 1978), of 3 kHz is used, as described previously (Vallurupalli et al. 2012). ^{15}N decoupling during t_2 is achieved using a 1 kHz WALTZ-16 field. ^{15}N chemical shift evolution during t_1 is recorded in a semi-constant time manner (Grzesiek and Bax 1993; Logan et al. 1993), with χ_1 and χ_2 set to max(T − t_1/2, 0) and max(0, t_1/2 − T) respectively. As described previously, CEST experiments are recorded as a set of 2D planes where the position of the weak B_1 field is varied; an additional plane is recorded with the CEST element removed so that R_1 values of spins in the ground state can be estimated robustly (Vallurupalli et al. 2012). In order to compensate for differential heating that would otherwise occur when this data set is recorded, a ^{1}H decoupling block (indicated in *parenthesis*) is inserted at the end of the sequence. Note that this block is removed when the CEST element is present (between gradients g4 and g5). **a** The ^{1}H and ^{15}N carriers are placed at water and 119 ppm respectively for the duration of the experiment. The ^{13}C carrier is placed initially at 58 ppm ($^{13}C^{\alpha}$) and subsequently positioned at 176 ppm (^{13}CO) immediately after gradient g6 for the remainder of the sequence. During the CEST period, the ^{13}C carrier is placed at distinct $13C^{\alpha}$ frequencies that are varied with each separately acquired ^{15}N, $^{1}H^{N}$ data set. $^{13}C^{\alpha}$ and ^{13}CO rectangular pulses are applied with fields of $\zeta/\sqrt{3}\,(180^{\circ})$ or $\zeta/\sqrt{15}\,(90^{\circ})$ Hz where ζ is the frequency difference in Hz between the centers of the $^{13}C^{\alpha}$ (58 ppm) and ^{13}CO (176 ppm) spectral regions (Kay et al. 1990). $^{13}C^{\alpha}$ decoupling is achieved using a WURST-2 adiabatic scheme (Kupce and Freeman 1996) with a bandwidth extending from 44 to 66 ppm and a maximum (rms) amplitude of 0.60 (0.36) kHz. $^{13}C^{\beta}$ decoupling makes use of a similar WURST-2 scheme extending from 19 to 46 ppm and from 68 to 72 ppm, with a maximum (rms) RF amplitude of 0.94 (0.42) kHz. When Gly-specific CEST experiments are recorded $^{13}C^{\beta}$ decoupling is not used and the value of τ_b set to 0.9 ms. Delays are: $\tau_a = 1.8$ ms, $\tau_b = 1.8$ ms, $\tau_c = 4$ ms, $\tau_d = 12.4$ ms, $\tau_e = 5$ ms, $\tau_f = 2.3$ ms, T = 12.4 ms, $\delta = 5.5$ ms and $\Delta = 0.5$ ms. The phase cycle is: $\phi_1 = (x,-x)$, $\phi_2 = 2(x), 2(-x)$, $\phi_3 = x$, receiver = $x,2(-x),x$. Gradient levels and durations (Gauss/cm; ms) are g1 = (16; 0.5), g2 = (−16; 0.5); g3 = (40; 1); g4 = (30; 1); g5 = (40; 1.5); g6 = (−10; 0.8); g7 = (−5,.5); g8 = (60; 1.25); g9 = (8; 0.3); g10 = (4; 0.4); g11 = (59.2; 0.125); g12 = (16, 1). Quadrature detection in F_1 is achieved using the gradient enhanced sensitivity method (Kay et al. 1992; Schleucher et al. 1993) whereby separate data sets are recorded with (ϕ3,g8) and (ϕ 3 + 180°,−g8). For each t_1 increment, ϕ_2 and the receiver phase are incremented by 180° (Marion et al. 1989). **b** The ^{1}H and ^{15}N carriers are placed at water and 119 ppm respectively, with the exception of during the CEST period when the position of the ^{1}H carrier is shifted to the center of the $^{1}H^{\beta}$ region. The ^{13}C carrier is initially placed at 43 ppm ($^{13}C^{\alpha/\beta}$), then shifted to a desired $^{13}C^{\beta}$ frequency for the CEST period, back to 43 ppm at the end of the CEST delay until immediately after gradient g6 where the carrier is jumped to 176 ppm (^{13}CO). Shaped $^{13}C^{\alpha/\beta}$ or ^{13}CO pulses are of the RE-BURP variety (~400 μs at 14.1 T) (Geen and Freeman 1991), with the green I-BURP pulse (1.8 ms, max B_1 of 2.95 kHz centered at 56.4 ppm, 14.1 T) (Geen and Freeman 1991) inverting $^{13}C^{\alpha}$ spins every other scan. All $^{13}C^{\alpha/\beta}$, $^{13}C^{\alpha}$ and ^{13}CO rectangular pulses are applied with fields of $\zeta/\sqrt{3}(180^{\circ})$ or $\zeta/\sqrt{15}\,(90^{\circ})$ Hz where ζ (Hz) corresponds to 133 ppm ($^{13}C^{\alpha/\beta}$ pulses) or 118 ppm ($^{13}C^{\alpha}$ or ^{13}CO pulses) (Kay et al. 1990). $^{13}C^{\alpha}$ decoupling is achieved using a WURST-2 adiabatic scheme, as in (A). Delays are: $\tau_a = 1.8$ ms, $\tau_b = 0.93$ ms, $\tau_c = 3.6$ ms, $\tau_d = 5$ ms, $\tau_e = 6$ ms, $\tau_f = 12.4$ ms, $\tau_g = 5$ ms, $\tau_h = 2.3$ ms, T = 12.4 ms, $\delta = 5.5$ ms and $\Delta = 0.5$ ms. The phase cycling is $\phi_1 = 2(x),2(-x)$, $\phi_2 = 4(x),4(-x)$, $\phi_3 = x$, receiver = $2(x),4(-x),2(x)$. Gradient levels and durations (Gauss/cm; ms) are g1 = (16; 0.5), g2 = (−16; 0.5); g3 = (40; 1); g4 = (30; 1); g5 = (40; 1.5); g6 = (−10; 0.8); g7 = (−20; 0.8); g8 = (60; 1.25); g9 = (8; 0.3); g10 = (−10; 0.4); g11 = (59.2; 0.125); g12 = (16; 1). Quadrature detection in F_1 is achieved using the enhanced sensitivity gradient method by recording a pair of data sets with (ϕ3,g8) and (ϕ 3 + 180°,−g8). For each successive complex t_1 point ϕ_2 and the phase of the receiver are incremented by 180°

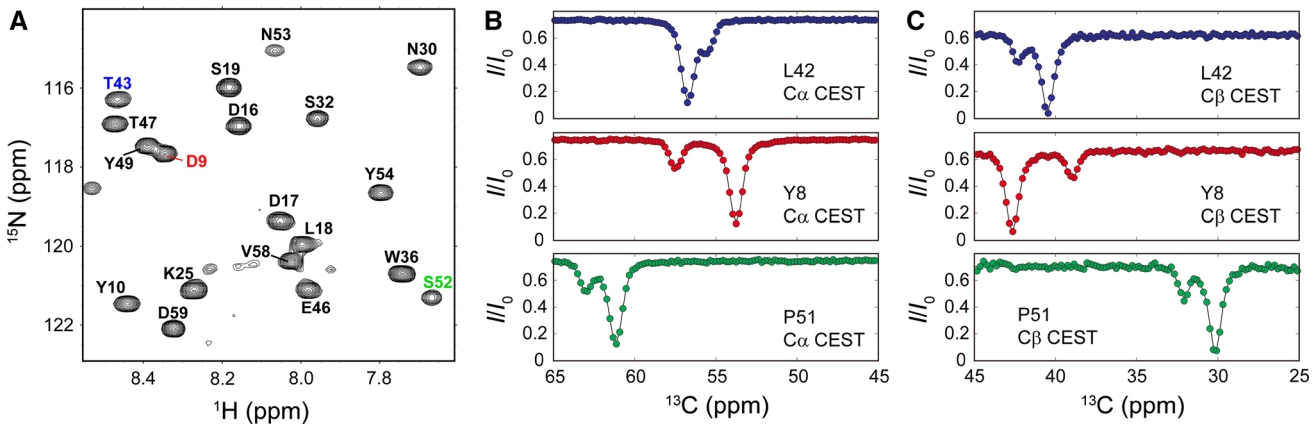

Fig. 2 Selected $^{13}C^{\alpha}$ and $^{13}C^{\beta}$ CEST profiles from HACACONNH- and HBCBCACONNH-based spectra. All experiments were recorded on a 2 mM sample of the G48A Fyn SH3 domain, U–[^{15}N, ^{13}C], 0.2 mM EDTA, 0.05 % NaN_3, 50 mM sodium phosphate (pH 7.0), 90 % H_2O/10 % D_2O, 25 °C, 14.1 T. Both data sets were acquired using a weak B_1 CEST field of 27 Hz, $T_{EX} = 125$ ms, 60 complex t_1 points and a recycle delay of 2 s. For the HACACONNH CEST data set the positions of the weak B_1 field were varied from 43.2 to 67.1 ppm with a spacing of 30 Hz (total measurement time of 37.5 h), while the HBCBCACONNH scheme used a range extending from 17.1 to 47.2 ppm and from 67.1 to 74.3 ppm with a spacing of 30 Hz for a total measurement time of 58.7 h. **a** Selected region of the 2D $^{1}H^{N}$–^{15}N HSQC spectrum of the G48A Fyn SH3 domain. Assignments of cross peaks are as indicated with the color-coding as in (**b**) and (**c**). Note that amide peaks from residue k are modulated according to the ^{13}C shifts of residue $k - 1$. All data were fit by numerical integration of the Bloch–McConnell equations (McConnell 1958), following a procedure described previously (Bouvignies et al. 2014). Fits to experimental data (*circles*) are shown by *solid lines*

in the context of HNCO derived CEST experiments probing exchange at ^{13}CO positions in proteins (Vallurupalli and Kay 2013), one bond ^{13}C–^{13}C couplings (51 Hz for $^{13}C^{\alpha}$–^{13}CO and 35 Hz for aliphatic ^{13}C spins) are not resolved for B_1 fields on the order of 25 Hz. In general the width of a dip is sensitive to the size of the B_1 field, the relaxation properties of the corresponding spin as well as the presence of scalar couplings that are typically unresolved in the CEST trace. For the experiments described here we recommend using fields on the order of 25 Hz, or larger, to avoid the appearance of unwanted multiplet components. It is noteworthy that the effects of all (unresolved) one-bond ^{13}C couplings have been included in our analyses of individual CEST profiles following an approach described previously (Bouvignies et al. 2014). We have also extracted exchange parameters, k_{ex} and p_E, where p_E is the fractional population of the excited state, corresponding to the unfolded conformer in the present case. These values, $k_{ex} = 134 \pm 3\ s^{-1}$, $p_E = 5.3 \pm 0.1$ % ($^{13}C^{\alpha}$) and $k_{ex} = 151 \pm 7\ s^{-1}$, $p_E = 5.1 \pm 0.1$ % ($^{13}C^{\beta}$) are in excellent agreement with $k_{ex} = 137 \pm 1\ s^{-1}$ and $p_E = 5.3 \pm 0.1$ % that were obtained from analysis of ^{15}N CEST data recorded on the same sample.

For both sets of experiments T_{EX} values of only 125 ms were used since, as can be seen from Fig. 2b,c, large dips could be observed at even relatively short mixing times. As such, I/I_o ratios [$I/I_o = \exp(-R_1 T_{EX})$], where I and I_o correspond to intensities of amide correlations in data sets recorded with and without the CEST period, respectively, are large. In principle, slow decay of magnetization during the CEST element is important to the success of the experiment because it improves sensitivity and in general extends the realm of application of the methodology to include systems that exchange more slowly. In this context, the schemes of Fig. 1 are advantageous over other approaches where the effective relaxation rates of magnetization during the CEST delay are larger. For example, in addition to the HACACONNH scheme of Fig. 1a, we have recorded $^{13}C^{\alpha}$ CEST profiles using an HNCOCA approach, Fig. S1. In this case the magnetization of interest during the CEST element is given by the operator, $4N_Z CO_Z C_Z^{\alpha}$, where X_Z is longitudinal magnetization from spin X and the effective relaxation rate can be approximated by $R_{1,eff} \sim R_{1,N} + R_{1,CO} + R_{1,C\alpha}$. In contrast, the term of interest during the CEST period in the scheme of Fig. 1a is, C_Z^{α}, with $R_{1,eff} = R_{1,C\alpha}$. The more favorable relaxation rates in the HACACONNH versus HNCOCA translate into significantly improved sensitivity for the former experiment, especially for larger T_{EX} values. Figure 3a plots the average of intensity ratios of cross peaks recorded in HNCOCA and HACACONNH data sets as a function of T_{EX} that clearly makes the point. Notably, average $R_{1,eff}$ values of 2.2 and 5.3 s^{-1} are obtained for the density elements of interest during the CEST interval in the HACACONNH and HNCOCA experiments, Fig. 3b. As an interesting aside, calculations show that the difference in $R_{1,eff}$ values decreases as a function of increasing molecular size because the relaxation of the longitudinal order term, $4N_Z CO_Z C_Z^{\alpha}$, does not contain spectral density contributions at zero frequency from dipolar ^{13}CO–$^{13}C^{\alpha}$ interactions, while the decay of C_Z^{α} does (Yamazaki et al. 1994). The

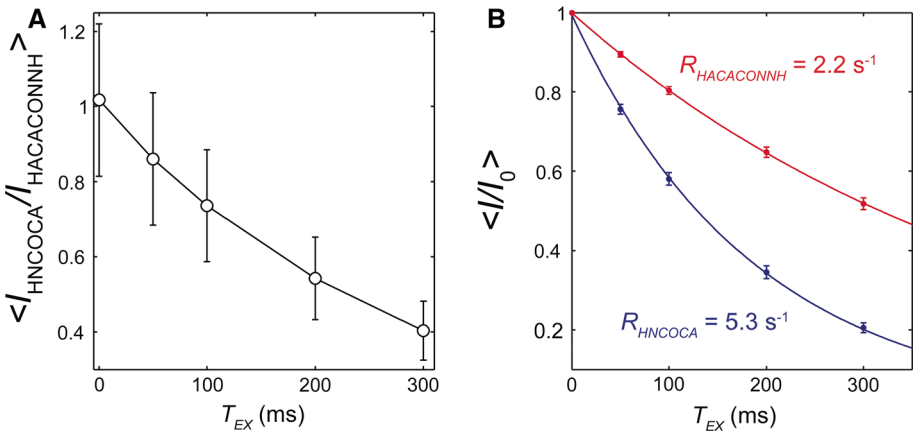

Fig. 3 Relative signal-to-noise ratios of correlations in HNCOCA and HACACONNH $^{13}C^{\alpha}$ CEST experiments as a function of T_{EX}. **a** Ratio of corresponding peak intensities in the data sets, averaged over all residues. *Error bars* indicate one standard deviation of the relative ratios of peak intensities in the two experiments. **b** Average intensities (I) of correlations in each of the HACACONNH (*red*) and HNCOCA (*blue*) experiments, normalized to the corresponding intensity in the absence of the CEST element (I_o). *Error bars* denote one standard deviation in intensity ratios of I and I_o. The decay of $<I/I_o>$ with T_{EX} provides an estimate of the average relaxation rates of the operative density elements during the CEST period, C_Z^{α} versus $4N_ZCO_ZC_Z^{\alpha}$. Note that the CEST field was placed far off resonance so as not to perturb the intensities of any of the correlations

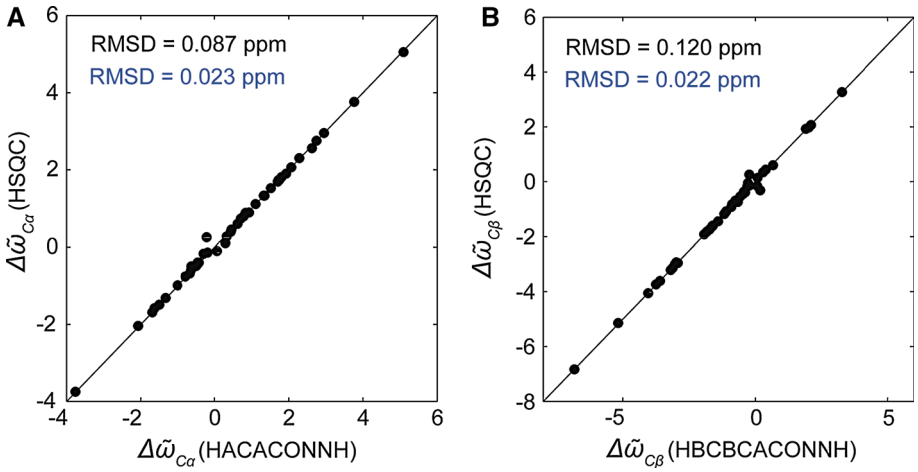

Fig. 4 Comparison of excited state $^{13}C^{\alpha}$ (**a**) and $^{13}C^{\beta}$ (**b**) chemical shifts extracted from HACACONNH- and HBCBCACONNH-based CEST experiments (X-axis) with those measured previously using a ^{13}C–^{1}H HSQC approach (Bouvignies et al. 2014). RMSD values (*black*) are calculated including all residues, while those in *blue* are for residues for which $|\Delta\varpi| > 1$ ppm

cross-over point depends on the static magnetic field at which the experiments are conducted, the CO CSA and the dynamic properties at each site but is predicted to occur for proteins tumbling with an effective correlation time on the order of 20–30 ns.

Figure 4 shows linear correlation plots of $\Delta\varpi$ $(\varpi_E - \varpi_G)$ values, where ϖ_I is the chemical shift of a spin in state I obtained via the methodology reported here (X-axis) and previously based on ^{13}C, ^{1}H HSQC experiments (Y-axis) (Bouvignies et al. 2014). Notably, excellent agreement is obtained, with RMSD values of approximately 0.1 ppm that decrease by fourfold–fivefold when $|\Delta\varpi|$ values greater than 1 ppm are considered.

In summary, we have presented ^{15}N, $^{1}H^{N}$-based triple resonance CEST experiments for recording $^{13}C^{\alpha}$ and $^{13}C^{\beta}$ chemical shifts of 'invisible' conformers that exchange with an observable ground state. As previously noted, the combination of $^{13}C^{\alpha}$ and $^{13}C^{\beta}$ shifts is particularly powerful for secondary structure prediction that forms the basis of any initial structural characterization (Han et al. 2011; Shen et al. 2009; Spera and Bax 1991; Wishart and Sykes 1994). Like other CEST experiments the methodology is most sensitive to systems exchanging with rates on the order of 500 s^{-1} or less and between states that are populated at a level of 1 % or higher (Bouvignies et al. 2014). The triple resonance CEST experiments and those based on the ^{13}C–^{1}H HSQC (Bouvignies et al. 2014) are complementary in the sense that they have unique strengths. For example, the experiments described here promise to be most useful for applications involving systems where resolution is limiting, such as for partially folded proteins or proteins in excess of approximately 100 residues for which

^{13}C–^{1}H HSQC data sets often become overlapped. By contrast, because the $^{13}C^{\alpha}$ CEST profiles can be recorded using non-CT HSQC experiments by using band selective $^{13}C^{\beta}$ decoupling during ^{13}C t_1 evolution (Bouvignies et al. 2014), the ^{13}C–^{1}H HSQC approach can be more sensitive than the HACACONNH based experiment. The choice of which experimental strategy to employ may, in many cases, reflect a tradeoff between sensitivity and resolution. The triple resonance CEST approach adds to an increasing list of powerful experiments that are finding use in characterizing sparsely populated conformers that are often critical for biological function.

Acknowledgments D.L. and A.S. are recipients of post-doctoral scholarships from the Canadian Institutes of Health Research (CHIR). This work was supported by a grant from the CIHR. L.E.K holds a Canada Research Chair in Biochemistry.

References

Bax A, Grzesiek S (1993) Methodological advances in protein NMR. Acc Chem Res 26:131

Bouvignies G, Vallurupalli P, Kay LE (2014) Visualizing side chains of invisible protein conformers by solution NMR. J Mol Biol 426:763–774

Cavanagh J, Fairbrother WJ, Palmer AG, Skelton NJ (1996) Protein NMR spectroscopy: principles and practice. Academic Press, San Diego

Clore GM, Gronenborn AM (1991) Structures of larger proteins in solution: three- and four-dimensional heteronuclear NMR spectroscopy. Science 252:1390–1399

Ernst RR, Bodenhausen G, Wokaun A (1987) Principles of nuclear magnetic resonance in one and two dimensions. Oxford University Press, Oxford

Geen H, Freeman R (1991) Band-selective radiofrequency pulses. J Magn Reson 93:93–141

Grzesiek S, Bax A (1992) Correlating backbone amide and side chain resonances in larger proteins by multiple relayed triple resonance NMR. J Am Chem Soc 114:6291–6293

Grzesiek S, Bax A (1993) Amino acid type determination in the sequential assignment procedure of uniformly 13C/15 N-enriched proteins. J Biomol NMR 3:185–204

Grzesiek S, Anglister J, Bax A (1993) Correlation of backbone amide and aliphatic side chain resonances in $^{13}C/^{15}N$ enriched proteins by isotropic mixing of ^{13}C magnetization. J Magn Reson Ser B 101:114–119

Han B, Liu Y, Ginzinger SW, Wishart DS (2011) SHIFTX2: significantly improved protein chemical shift prediction. J Biomol NMR 50:43–57

Kay LE, Ikura M, Tschudin R, Bax A (1990) Three-dimensional triple-resonance NMR spectroscopy of isotopically enriched proteins. J Magn Reson 89:496–514

Kay LE, Keifer P, Saarinen T (1992) Pure absorption gradient enhanced heteronuclear single quantum correlation spectroscopy with improved sensitivity. J Am Chem Soc 114:10663–10665

Kupce E, Freeman R (1996) Optimized adiabatic pulses for wideband spin inversion. J Magn Reson Ser A 118:299–303

Levitt M, Freeman R (1978) NMR population inversion using a composite pulse. J Magn Reson 33:473–476

Logan TM, Olejniczak ET, Xu RX, Fesik SW (1993) A general method for assigning NMR spectra of denatured proteins using 3D HC(CO)NH-TOCSY triple resonance experiments. J Biomol NMR 3:225–231

Long D, Bouvignies G, Kay LE (2014) Measuring hydrogen exchange rates in invisible protein excited states. Proc Natl Acad Sci USA 111:8820–8825

Marion D, Ikura M, Tschudin R, Bax A (1989) Rapid recording of 2D NMR spectra without phase cycling. Application to the study of hydrogen exchange in proteins. J Magn Reson 85:393–399

McConnell HM (1958) Reaction rates by nuclear magnetic resonance. J Chem Phys 28:430–431

Montelione GT, Lyons BA, Emerson SD, Tashiro M (1992) An efficient triple resonance experiment using carbon-13 isotropic mixing for determining sequence-specific resonance assignments of isotopically-enriched proteins. J Am Chem Soc 114:10974–10975

Santoro J, King GC (1992) A constant-time 2D overbodenhausen experiment for inverse correlation of isotopically enriched species. J Magn Reson 97:202–207

Sattler M, Schleucher J, Griesinger C (1999) Heteronuclear multidimensional NMR experiments for the structure determination of proteins in solution employing pulsed field gradients. Prog Nucl Magn Reson Spectrosc 34:93–158

Schleucher J, Sattler M, Griesinger C (1993) Coherence selection by gradients without signal attenuation: application to the three-dimensional HNCO experiment. Angew Chem Int Ed Engl 32:1489–1491

Shaka AJ, Keeler J, Frenkiel T, Freeman R (1983) An improved sequence for broadband decoupling: WALTZ-16. J Magn Reson 52:335–338

Shen Y, Delaglio F, Cornilescu G, Bax A (2009) TALOS+: a hybrid method for predicting protein backbone torsion angles from NMR chemical shifts. J Biomol NMR 44:213–223

Spera S, Bax A (1991) Emperical correlation between protein backbone conformation and c-alfa and c-beta c13 nuclear magnetic resonance chemical shifts. J Am Chem Soc 113:5490–5492

Vallurupalli P, Kay LE (2013) Probing slow chemical exchange at carbonyl sites in proteins by chemical exchange saturation transfer NMR spectroscopy. Angew Chem Int Ed Engl 52:4156–4159

Vallurupalli P, Bouvignies G, Kay LE (2012) Studying 'invisible' excited protein states in slow exchange with a major conformation. J Am Chem Soc 134:8148–8161

Vuister GW, Bax A (1992) Resolution enhancement and spectral editing of uniformly ^{13}C-enriched proteins by homonuclear broadband ^{13}C decoupling. J Magn Reson 98:428–435

Wishart DS, Sykes BD (1994) The ^{13}C chemical-shift index: a simple method for the identification of protein secondary structure using ^{13}C chemical-shift data. J Biomol NMR 4:171–180

Wittekind M, Mueller L (1993) HNCACB, a high sensitivity 3D NMR experiment to correlate amide proton and nitrogen resonances with the alpha- and beta-carbon resonances in proteins. J Magn Reson Series B 101:201–205

Yamazaki T, Muhandiram R, Kay LE (1994) NMR experiments for the measurement of carbon relaxation properties in highly enriched, uniformly ^{13}C, ^{15}N labeled proteins: application to $^{13}C^{\alpha}$ carbons. J Am Chem Soc 116:8266–8278